J. MATER. CHEM., 1991, 1(4), 511–515

X-Ray Diffraction Characterization of Iridium Dioxide Electrocatalysts

Alvise Benedetti,*[a] Stefano Polizzi,[a] Pietro Riello,[a] Achille De Battisti[b] and Andrea Maldotti[b]
[a] *Dipartimento di Chimica Fisica, Calle Larga S. Marta 2137, I-30123 Venezia, Italy*
[b] *Dipartimento di Chimica dell'Università and Centro di Studio sulla Fotochimica e Reattività degli Stati Eccitati C.C. del C.N.R., via L. Borsari 46, I-44100 Ferrara, Italy*

An X-ray diffraction (XRD) line-broadening analysis of coatings of pyrolytic iridium dioxide supported on amorphous silica microbeads is reported. The influence of the temperature of pyrolysis and of the annealing treatments on the average crystallite sizes of the IrO_2 and Ir phases have been studied in detail. The values obtained for IrO_2 are lower than those obtained from an analgous RuO_2 system. However, the analysis suggests that in both cases the crystalline phase grows within an amorphous microcrystalline environment where impurities are mostly segregated in the amorphous phase and then released to the atmosphere. The lattice parameters are also calculated. Compared with the reference values, slightly greater values are obtained both for IrO_2 and for Ir.

Keywords: *X-Ray diffraction*; *Line broadening*; *Iridium dioxide*; *Electrocatalyst*

The industrial interest of pyrolytic oxides of ruthenium and iridium has stimulated many works on the electrochemistry of these synthetic materials since the early 1970s. The literature on fundamental and industrial aspects has been thoroughly discussed in several reviews[1–4] and the influence of annealing temperatures of ruthenium oxide electrodes on the microstructural features was recognized by Pizzini *et al.* in one of the first papers.[5] The same aspect was implicitly taken into account in other pioneering works,[6–8] where the electrochemical charging mechanism of this material has been studied.

Analogous investigations were carried out later on iridium dioxide, for which precursor paths and microstructural features have also been discussed.[9–14] Generally, the microstructural texture of RuO_2 and IrO_2 affects their electrochemical properties in different ways. The surface area or the roughness factor substantially reflects the crystallite size which is related to the 'degree of dispersion' of the material. In this sense, not only the catalytic activity, but also the resistance to corrosion under applied potential may be modified by changing the microstructure of the oxides. This aspect, directly correlatable with the preparation path, is probably the most widely considered in the literature.[1,2,9] Moreover, the presence of lattice distortions can also exert a basic effect on the chemical behaviour of the material: a large number of microstructural defects can be related, in principle, to a larger number of active sites.

In this context the analysis of the line-broadening of XRD peaks has proven to be extremely useful for the microstructural characterization of crystalline phases. However, the simplified approaches generally used in the characterization of RuO_2 and IrO_2 films,[1,6] which are based on the measurement of the apparent crystallite size calculated by the Scherrer equation, have limited the potential of this approach.

In the present work a careful XRD line-broadening analysis on coatings of pyrolytic iridium dioxide supported on amorphous silica microbeads is presented. In a previous study, the formation of iridium metal, together with the expected oxide was discussed on the basis of XRD phase identification and thermoanalytical data.[10] In the same work an analysis of the effect of temperature of pyrolysis and temperature and duration of the annealing treatments was also carried out. The complexity of the transformations that the film undergoes during the different thermal treatments[10,11] has prompted a more detailed XRD investigation.

In particular, a Fourier line-broadening analysis of XRD peak profiles, and, if possible, the Warren–Averbach (W–A) method[15] allow a careful microstructural analysis of the different phases in order to obtain average crystallite sizes, crystallite size distributions and lattice distortions possibly present. Usually this approach, for which a complete knowledge of the peak profiles on a large portion of reciprocal space is necessary, is limited by the presence of very broadened peak envelopes and/or of an important or complex background. In order to overcome this problem a 'profile fitting technique' has been used, in which one fits the experimental envelopes of peaks with analytical functions [one for the background and two for each profile ($K\alpha_1 + K\alpha_2$)] utilizing a minimization routine. Previous tests on different materials[16,17] showed that it is possible to obtain very reliable results in spite of some simplifications and theoretical assumptions.

Experimental and Methodology

Samples Preparation

The samples investigated were prepared by painting amorphous silica microbeads (spherosil) with isopropyl alcohol solutions of hydrated iridum(III) chloride, followed by evaporation of the solvent under controlled conditions.[10] The final coatings were obtained by pyrolysis at 673 K for 2 h, and by successive annealing at 673, 773 and 873 K for periods of 15 h and at 673 K for 30 and 58 h, respectively. Both pyrolysis and annealing were performed under dry oxygen. In such a way we were able to analyse the influence of the temperature and of the time of annealing on the microstructural features of the developed components.

Wide-angle X-Ray Scattering (WAXS)

Profiles were collected using a Philips vertical goniometer connected to a highly stabilized generator. Cu-Kα Ni-filtered radiation, a graphite monochromator and a proportional counter with a pulse-height discriminator were used. A step-by-step technique was employed; steps were of 0.05° with an accumulation counting time of 100 s per angular abscissa.

Line-broadening Analysis

For each peak, two pseudo-Voigt functions (linear combination of a Gaussian profile with a Cauchian one) related by the well known crystallographic constraints on peak intensities, angular positions and half-width at half-maximum were used in order to take account of the $K\alpha_1$–$K\alpha_2$ doublet.[16] For the background, a straight line or a polynomial of the third degree was used, depending on the angular range under consideration. The minimization was carried out using a modified version of the Simplex method.[18] The optimized pseudo-Voigt functions relevant to the $K\alpha_1$ of the experimental broadened profile were deconvoluted from the instrumental and spectral effects in order to obtain the corrected Fourier transforms $A(L)$ (L is the variable in direct space).[19] According to Warren and Averbach the coefficients $A(L)$ (or the Fourier transforms) are the products of size coefficients $A_s(L)$ and distortion coefficients $A_d(L)$:

$$A(L)=A_s(L)A_d(L)$$

where $A_s(L)$ is independent of the peak order and $A_d(L)$ is dependent upon the order of the diffraction peak. If at least two orders of reflections of the same plane family are known, by means of the following expression:

$$\ln A\ (L,1/d_{hkl}^2)=\ln A_s(L)-2\pi^2\langle\varepsilon^2(L)\rangle L^2/d_{hkl}^2 \qquad (1)$$

where hkl are the Miller indices, $\langle\varepsilon^2(L)\rangle$ is the squared microstrain averaged over all distances L, and d_{hkl} is the interplanar spacing, it is possible to separate the crystallite size contribution from that of the lattice distortion. Furthermore, it has been shown that the volume-weighted crystalline size distribution, $p_v(L)$, obeys the following relation

$$p_v(L)\propto L[\mathrm{d}^2A_s(L)/\mathrm{d}L^2] \qquad (2)$$

while the volume-weighted average crystallite size $\langle D\rangle_v$ calculated perpendicular to the (hkl) planes is given by

$$\langle D\rangle_v=\int_0^\infty Lp_v(L)\mathrm{d}L\Big/\int_0^\infty p_v(L)\mathrm{d}L \qquad (3)$$

Only the peaks in the range between 10 and 50° in 2θ and the 202 IrO_2 peak at *ca.* 73° were examined. For the other profile envelopes it was not possible to obtain an unambiguous and stable solution for the very broadened constituent reflections. Moreoever, owing to the variable values of the unit cell parameters of the crystalline phases considered (see Table 3, later), it was not possible to fix, *a priori*, some 'known' parameters in the fitting procedure, at the position of the maximum of the peaks, in order to diminish the number of parameters to minimize.

In order to describe the decreasing background scattering of the amorphous silica, a polynomial of the third degree was considered for the 2θ range *ca.* 24–45°. This simplification was necessary in the fitting procedure because no suitable scaling factor of the 'true' experimental amorphous background, scattered by the microbeads, could be found. Even if this fact could be explained by interference effects, the contribution of a non-crystalline phase containing Ir cannot be excluded. For narrower ranges a straight line was found sufficient to reproduce the background.

Results

The spectra of the five different samples are characterized by a big halo centred at about $2\theta=22°$, due to the amorphous silica, and by the presence of two different crystalline phases, IrO_2 (rutile structure) and Ir. As already described in our previous paper, the higher the annealing temperature the smaller the amount of iridium present, whereas the amount of iridium was almost constant for different times of isothermal treatment.[10]

In Fig. 1 we report, as an example, the X-ray pattern of the sample annealed at 673 K for 30 h. From the figure, and inset, it is evident that the presence of the background and the overlaps makes the use of the 'profile-fitting technique' necessary in order to apply Fourier X-ray analysis. In this way, it has been possible to study the 110, 101, 200 and 202 reflections relevant to the IrO_2 phase and the 111 and 200 reflections relevant to the Ir phase. In Fig. 2 the fitting of the

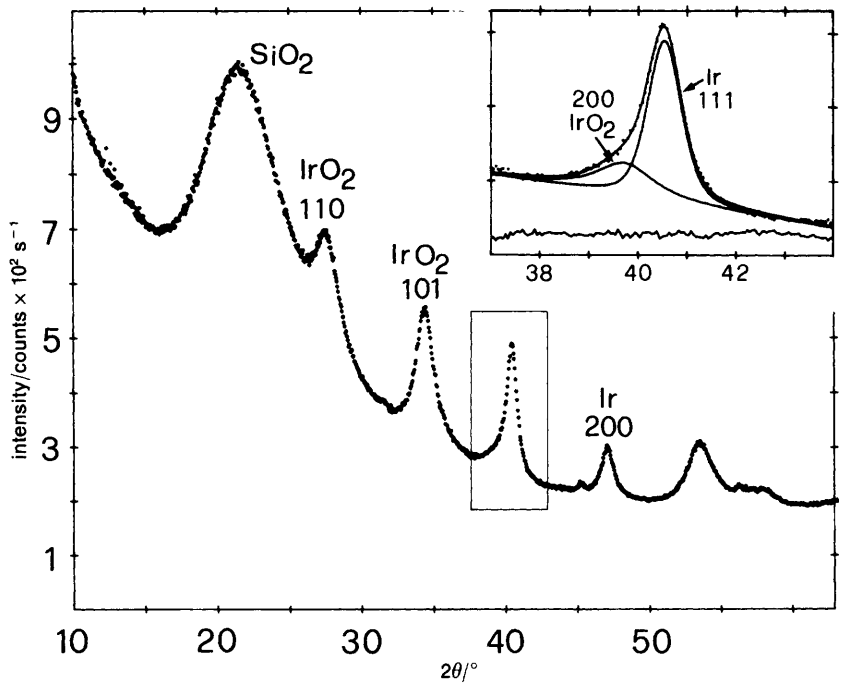

Fig. 1 XRD pattern of the sample annealed at 673 K for 30 h. The inset shows the best-fitted envelope of the 200 IrO_2 and the 111 Ir profiles with the corresponding residuals

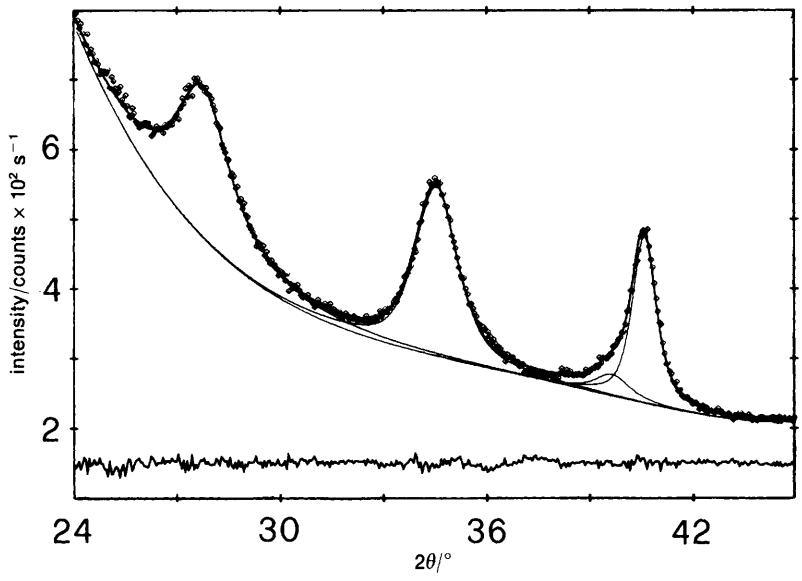

Fig. 2 Experimental data (dots) and fitting (continuous line) of the envelope of the amorphous component; the 110, 101 and 200 IrO_2 and 111 Ir profiles relevant to the sample annealed at 673 K for 58 h. Residuals are reported below

IrO_2 110, 101, 200 and the Ir 111 profiles, together with the amorphous component, is shown for the sample annealed at 673 K for 58 h.

The index used was

$$R_{wp}=\left\{\sum_i w_i[I_{fit}(2\theta_i)-I_{obs}(2\theta_i)]^2 \Big/ \sum_i w_i I_{obs}(2\theta_i)^2\right\}^{1/2}$$

where $w_i=1/[I_{obs}(2\theta_i)]$ is the weight assigned to the ith observation, $I_{fit}(2\theta_i)$ and $I_{obs}(2\theta_i)$ are the calculated and observed profile intensities at $2\theta_i$. The obtained R_{wp} values (<2.0%), indicate that the fitted analytical envelope reproduces the experimental X-ray pattern in a satisfactory way.

The W–A method has been applied to the 101 and 202 IrO_2 peak profiles. In Fig. 3 the relevant Fourier coefficients for the sample annealed at 873 K for 15 h are shown. The inset shows the corresponding Warren–Averbach diagram. The slopes of the straight lines in this diagram are related to the strain parameter, according to eqn. (1): negative values indicate the presence of strain. The slopes shown in Fig. 3 are nearly zero within the errors involved in this procedure, so that this kind of disorder can be considered negligible. Similar results have been obtained for the other samples. This confirms that no strain is present in the IrO_2 crystalline phase.

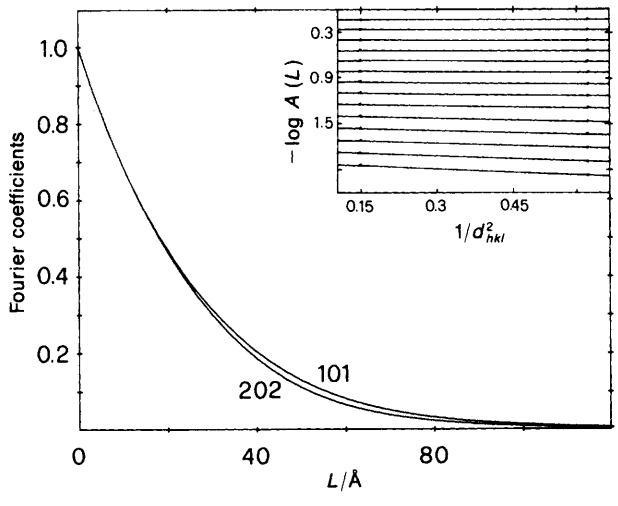

Fig. 3 $A(L)$ Fourier coefficients for the 101–202 pair of reflections for the sample annealed at 873 K for 15 h. Inset: Warren-Averbach diagram in which the logarithms of $A(L)$ are reported as functions of $1/d_{hkl}^2$ ($\Delta L=3.56$ Å)

Table 1 shows the values of the volume-weighted average crystallite sizes obtained from each peak. The Fourier analysis of profiles 110 and 200 is further evidence of the absence of strain. In fact, for these two profiles, although all the broadening has been attributed only to the crystallite size, the resulting average crystallite sizes are similar to the ones obtained by applying the W–A method. The fact that the crystallite sizes calculated from the different analysed profiles of the same sample are very similar, indicates that IrO_2 crystallites can be considered equiaxial in three-dimensional space.

The last column of Table 1 reports the average of the volume-weighted average crystallite sizes of the four profiles, D. The duration of the annealing treatment has no effect on the IrO_2 crystallite size. As far as the effect of the annealing temperature is concerned, the increase of $\langle D\rangle_v$ from 673 to 873 K can be considered larger than the relevant estimated error (10–15%).

The role of the different pyrolysis temperature is shown in Fig. 4. The volume-weighted crystallite size distribution obtained according to eqn. (2) for the 101 reflection for the sample annealed at 873 K [curve (*a*)] and that obtained directly by pyrolysis of the precursor salt at 873 K [curve (*b*)] are reported. The different pyrolysis temperature affects the crystallite size quite significantly.

The behaviour of the iridium crystalline phase under heat treatment is rather different. In Table 2 the $\langle D\rangle_v$ values are reported. Both the time of isothermal annealing and the annealing to higher temperature have the effect of increasing the iridium crystallite size. The difference obtained for the two considered crystallographic directions could be due to a preferential direction of growth of the crystallites. However, owing to the lack of further peaks for analysis and to the large amorphous contribution the problem has no definite solution.

The application of the fitting procedure also has the advantage that it supplies the values of the position of the peak maximum with very high precision, allowing one to obtain accurate lattice parameters. Table 3 shows the values of the IrO_2 and Ir unit-cell parameters, obtained with a computer

Table 1 Average crystallite sizes calculated from different *hkl* profiles relevent to the IrO_2 phase

annealing temperature/K	time/h	average crystallite size $\langle D\rangle_v$/Å			
		W–A pair 101–202	110	200	$\bar{D}$/Å
673	15	37	41	43	40
673	30	40	42	36	39
673	58	38	48	43	43
773	15	41	46	51	46
873	15	54	55	45	51

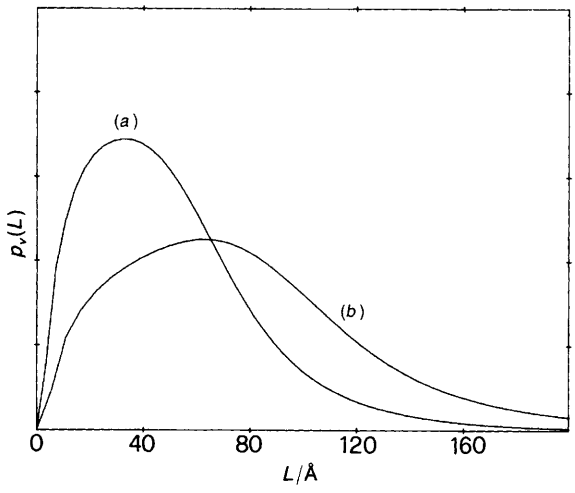

Fig. 4 Volume-weighted crystalline size distributions $p_v(L)$, calculated from the 101 reflection, relevant to the sample annealed at 873 K for 15 h [curve (*a*) $\langle D\rangle_v = 51$ Å] and to the sample obtained directly by pyrolysis of the precursor salt at 873 K [curve (*b*) $\langle D\rangle_v = 80$ Å]

Table 2 Volume-weight average crystallite sizes calculated from the 111 and 200 profiles relevant to the Ir phase

annealing temperature/K	time/h	average crystallite size $\langle D\rangle_v$/Å	
		111	200
673	15	94	72
673	30	115	72
673	58	124	87
773	15	113	79
873	15	153	133

Table 3 Unit-cell parameters relevant to the tetragonal IrO_2 and cubic Ir phases

annealing temperature/K	time/h	IrO_2		Ir a_o/Å
		a_o/Å	c_o/Å	
673	15	4.544(3)	3.175(5)	3.859(3)
673	30	4.505(3)	3.183(5)	3.853(3)
673	58	4.497(4)	3.178(2)	3.846(2)
773	15	4.533(6)	3.165(3)	3.853(4)
873	15	4.522(6)	3.162(3)	3.850(3)
Lit.[20]		4.4983	3.1544	3.8394

refinement programme for the different samples. In general, compared with the reference values,[20] slightly greater values are obtained both for the IrO_2 and for Ir. In any case, when the time or the temperature are increased the values approach the standard ones. This fact could suggest that, after the thermal and the annealing treatment, neither crystalline phase is easily reproducible owing to the presence of substitutional ions in the structure.

Discussion and Conclusions

The relatively low $\langle D\rangle_v$ values of the IrO_2 crystallites yield a larger dispersion of the crystalline part of the IrO_2 catalyst compared to that obtained for an analogous RuO_2 system.[12] In this case, an average crystallite size up to 1500 Å was found under the same preparation conditions. However, in order to propose a possible explanation of this different behaviour, it is necessary to consider other aspects of analogous IrO_2 systems reported in previous papers.

Chemical analysis,[10] for instance, indicates that larger amounts of residual water and chlorine species are present in pyrolitic iridium oxide films compared with ruthenium oxide films prepared at the same temperature from the respective hydrated chlorides.[11] Thermal analysis confirms this result.[10] Hydrogen profiles obtained by the $^1H(^{15}N,\alpha\gamma)^{12}C$ nuclear reaction for RuO_2 and IrO_2 films[12] indicate that hydrogen species are stored in larger amounts in the IrO_2 samples. The average oxygen stoichiometry, found by Rutherford backscattering spectrometry was 2.5 for IrO_2 and 1.8 for RuO_2[12,13]. Moreover, in these systems, the RuO_2 and the IrO_2 crystalline phases grow from a pre-existing amorphous phase,[14] and for the RuO_2 with lattice parameters closely related to the temperature of annealing and chloride content:[5,21] the higher the temperature the closer the lattice parameters are to the reference values. On the basis of these results, it seems reasonable to assume that the crystalline rutile phase, common to both RuO_2 and IrO_2, grows within an amorphous microcrystalline environment where impurities are mostly segregated in the amorphous phase and then released into the surroundings. This stage seems to be quite slow in the case of the iridium dioxide films and powders, thus preventing further growth of IrO_2 crystallites, e.g. during the annealing treatments. Only direct pyrolysis at higher temperatures allows the achievement of larger crystallite size as shown in Fig. 4. For this system, the different values of lattice parameters are influenced by the temperature and the annealing time, however, no direct influence of the chloride ions has been detected.

As has already been outlined, as far as the Ir phase is concerned, we have not been able to evaluate the disorder influence, nor consequently to clarify the role of the impurities. In any case, the variation of the unit-cell parameters seems to suggest a 'true' decrease of a_o as a function of the annealing treatment.

The results obtained on the microstructure of IrO_2 films are also interesting from the electrochemical point of view. In fact, as mentioned in the introduction, the electrocatalytic activity of oxide electrodes, and their instability in relation to corrosion processes taking place under polarization, are linked by the ion-insertion characteristics of these materials. Accord-

ing to the evidence obtained in this work, the IrO_2 crystallites show no strain, which should minimize ion-exchange processes across them, so limiting the ions' mobility. The intergranular region, on the other hand, is likely to be quite large and, owing to its defective nature, could allow larger diffusion coefficients for small ions such as protons, that are involved in the charge-storage mechanism. IrO_2 electrodes prepared by the above-mentioned method in fact show large charge-storage capacity, compared with RuO_2 electrodes.[13]

We are grateful to Professor G. Fagherazzi for his constructive criticism and to Mr. L. Bertoldo for assistance during experimental work. This research work was supported by CNR (Progetto Finalizzato Materiali Speciali per Tecnologie Avanzate) and by Ministero dell'Università e della Ricerca Scientifica (MURST 40%).

References

1 S. Trasatti and G. Lodi, in *Electrodes of Conductive Metal Oxides*, ed. S. Trasatti, Elsevier, Amsterdam, 1980, part A, p. 301.
2 S. Trasatti and G. Lodi, in *Electrodes of Conductive Metal Oxides*, ed. S. Trasatti, Elsevier, Amsterdam 1981, part B p. 521.
3 A. Nidola, in *Electrodes of Conductive Metal Oxides*, ed. S. Trasatti, Elsevier, Amsterdam, 1981, Part B p. 627.
4 D. M. Novak, B. V. Tilak and B. E. Conway, in *Modern Aspects of Electrochemistry*, ed. B. E. Conway and J. Bockris, Plenum Press, New York, 1982, vol. 14, p. 195.
5 S. Pizzini, G. Buzzanca, C. Mari, L. Rossi and S. Torchio, *Mater. Res. Bull.*, 1972, **7**, 449.
6 G. Lodi, G. Zucchini, A. De Battisti, E. Sivieri and S. Trasatti, *Mater. Chem.*, 1978, **3**, 179.
7 S. Trasatti and G. Buzzanca, *J. Electroanal. Chem.*, 1971, **29**, 1.
8 G. Lodi, E. Sivieri, A. De Battisti and S. Trasatti, *J. Appl. Electrochem.*, 1978, **8**, 135.
9 C. Angelinetta, S. Trasatti, L. J. Atanososka, Z. S. Minevski and R. T. Anatososki, *Mater. Chem. Phys.*, 1989, **22**, 231.
10 G. Lodi, A. De Battisti, A. Benedetti, G. Fagherazzi and J. Kristof, *J. Electroanal. Chem.*, 1988, **256**, 441.
11 G. Lodi, A. De Battisti, G. Bordin, C. De Asmundis and A. Benedetti, *J. Electroanal. Chem.*, 1990, **277**, 139.
12 G. Battaglin, A. Carnera, G. Della Mea, G. Lodi and S. Trasatti, *J. Chem. Soc., Faraday Trans.* 1, 1985, **81**, 2995.
13 G. Lodi, G. L. Wucchini, A. De Battisti, A. Giatti, G. Battaglin and G. Della Mea, *Surf. Sci*, submitted.
14 I. D. Belova, T. V. Varlamova, B. Sh. Galyamov, Yu. E. Roginskaya, R. R. Shifrina, S. G. Prutchenko, G. I. Kaplan and M. A. Sevostyanov, *Mater. Chem. Phys.*, 1988, **20**, 39.
15 B. E. Warren, and *X-Ray Diffraction*, Addison-Wesley, Reading, MA. 1969, p. 264.
16 S. Enzo, S. Polizzi and A. Benedetti, *Z. Kristallogr.*, 1985, **170**, 275.
17 A. Benedetti, G. Fagherazzi, S. Enzo and M. Battagliarin, *J. Appl. Crystallogr.*, 1988, **21**, 543.
18 J. A. Nelder and R. Mead, *Comput. J.*, 1965, **7**, 308.
19 S. Enzo, G. Fagherazzi, A. Benedetti and S. Polizzi, *J. Appl. Crystallogr.*, 1988, **21**, 536.
20 Joint Committee on Powder Diffraction Standards, 1988, Powder Diffraction File (Swarthmore, Pennsylvania: International Centre for Diffraction Data) no. 6-0598 and 15-870.
21 G. Lodi, C. Bighi and C. De Asmundis, *Mater. Chem.*, 1976, **1**, 177.

Paper 0/05257D; *Received* 22*nd November*, 1990